Geotech Geol Eng
https://doi.org/10.1007/s10706-021-01951-4

ORIGINAL PAPER

Surficial Stabilization of Wildfire-Burnt Hillslopes Using Xanthan Gum and Polyacrylamide

Idil Deniz Akin · Sophia S. Garnica · Peter R. Robichaud · Robert E. Brown

Received: 23 July 2020 / Accepted: 22 July 2021

Abstract Post-wildfire erosion and the slope instability issues associated with it are a global problem that can negatively affect transportation corridors, the environment, and human life. Currently, mulch treatments are commonly used means of stabilizing wildfire-burnt hillslopes; however, mulch, especially agricultural straw mulch, can pose environmental concerns related to invasive plants. An environmentally friendly treatment, xanthan gum (XG), and a commercial polyacrylamide (PAM) were evaluated as alternatives for stabilizing surficial silty soil that was burnt by the 2018 Mesa Fire in central Idaho to reduce runoff-dominated erosion. Indoor rainfall experiments were conducted to simulate three wet-dry cycles. Runoff and infiltration were measured after each wetting and drying event, and used to compare the effectiveness of the admixture. The total runoff at the end of three wetting events increased slightly, by $\sim$ 4% for PAM and $\sim$ 12% for XG. These results indicate that both PAM and XG decrease soil loss and infiltration, but that neither seals the soil surface completely. The soil loss during each wetting event was found to be dependent on the water content before wetting and the corresponding regime in the soil water retention curve. PAM and XG maintained the unsaturated state in soil, with water contents consistently around 30% before the second and third wetting events. This resulted in similar runoffs and statistically significant reductions in soil loss. At the end of three events, the soil loss was reduced by 2.9 times for XG and 6.9 times for PAM, compared to the soil loss from untreated soil.

Keywords Erosion · Wildfire · Water retention · Xanthan gum · Polyacrylamide

I. D. Akin (✉) · S. S. Garnica
Department of Civil and Environmental Engineering, Washington State University, Pullman, WA 99164, USA
e-mail: idil.akin@wsu.edu

P. R. Robichaud · R. E. Brown
US Department of Agriculture, Forest Service, Rocky Mountain Research Station, Moscow, ID 83843, USA

1 Introduction

The western U.S. experiences large wildfires almost every summer, and these have been increasing in both size and frequency in recent decades (Westerling et al. 2006; Dennison et al. 2014; Westerling 2016). After a wildfire, the loss of vegetation biomass, especially on the soil surface, can greatly reduce the stability of soil (Robichaud 2005; Wagenbrenner et al. 2006). In Washington State and Idaho, wildfires are typically followed by rainfall in the fall or snow in the winter. Therefore, in addition to the immediate loss of life, property and habitat due to wildfires, slopes burnt by

Published online: 27 July 2021

wildfires with high soil burn severity pose a danger because they are more susceptible to surficial stability issues such as runoff-dominated surface erosion, precipitation-induced shallow landslides, and debris flows (e.g., Cannon et al. 2003; Robichaud et al 2013a, b; Staley et al. 2017).

Surficial stability issues result in both economic and environmental impacts and in some cases threaten human life. When sediment moves into stream channels, culverts may become blocked and roads may be washed out, which can lead to long-term road closures and therefore to significantly reduced system mobility (e.g., Foltz et al. 2009; Robichaud et al. 2000). Excess stream sediment may have adverse effects on aquatic life. For example, in the Pacific Northwest, salmon experience increased mortality rates, reduced growth rates, reduced resistance to disease, interference in egg development when nesting areas are clogged, and reduced availability of food due to the clogging of stream bottom interstitial spaces (Newcombe and MacDonald 1991; Smith and Caldwell 2001).

Erosion after wildfires is typically associated with a loss of ground cover protecting the soil surface and the creation of water-repellent soil conditions (Robichaud et al. 2016). A water-repellent layer is often formed a few centimeters below the surface if vapor from burned organics, which are hydrophobic, condenses below the surface with the development of a thermal gradient (e.g., Doerr et al. 2000; DeBano 2000). During rainfall events, the soil above the water-repellent layer becomes saturated. Since there is little downward drainage, pore water pressures increase and the soil above the water-repellent layer is prone to surface erosion and debris flow initiation, with rills forming within meters of hillslope crests (Staley et al. 2014; Wells 1987; Gabet 2003). Debris flows triggered by runoff-dominated erosion are a common stability issue after a wildfire (Cannon et al. 2003; Staley et al. 2017). In a 2005 study, 88% of reported debris flow events post wildfire were found to be due to runoff-dominated erosion (Gartner et al. 2005).

Another direct effect of a wildfire that is associated with erosion is a heat pulse though the upper soil profile. This causes loss of (1) microbial and fungal cohesion, cohesion due to precipitates of minerals such as calcium carbonate and iron oxide, and cohesion due to organics such as carbohydrates (e.g., Parise and Cannon 2012; Neary et al. 1999; Shakesby and Doerr 2006; Mataix-Solera et al. 2011; Lax and Garcia-Orenes 1993) and (2) clay structure and fine content because of the removal of OH^- groups at high (460 °C) temperatures (e.g., DeBano et al. 1998; Neary et al. 1999; Wondzell and King 2003; Durgin 1985; Mills and Fey 2004).

To reduce erosion and associated threats to downstream property, human life, transportation corridors, and aquatic habitat, critical slopes are stabilized after a wildfire (Robichaud and Ashmun 2013). The typical methods of stabilization are currently mulch treatments and seeding for vegetation regrowth (e.g., Robichaud et al. 2013a; Peppin et al. 2011). Mulch can be either dry mulch, which can be composed of rice and wheat straw or of wood shreds or wood strands, or hydromulch, which is typically a suspension of dry mulch, tackifier, suspension agent and seeds (e.g., Riechers et al. 2008; Wohlgemuth et al. 2011; Robichaud et al. 2013a). Polyacrylamide (PAM) treatment has also been used for erosion control, but in unburned agricultural and forest lands (e.g., Lentz and Sojka 1994). Studies found that PAM treatment increases aggregation in soils without sealing the soil surface or reducing the hydraulic conductivity (e.g., Terry and Nelson 1986; Bryan 1992; Shainberg et al. 1990). Most recently, biopolymers such as xanthan gum have been shown as potential alternatives for soil stabilization to prevent wind or runoff-dominated erosion of (e.g., Kavazanjian et al. 2009; Movasat and Tomac 2020), however, the impact of treatment on infiltration rate has not been evaluated.

This study evaluates the application of an environmentally friendly admixture, xanthan gum (XG), and a commercially available polyacrylamide (PAM), for surficial stabilization of a simulated burnt hillslope using soils collected after the 2018 Mesa Fire near Council, Idaho. Total runoff and soil loss were measured during three wet–dry cycles simulated with indoor rainfall experiments to evaluate the effectiveness of the XG and PAM treatments at the same application rate (percent dry mass) and an untreated control.

2 Study Site and Sample Collection

The Mesa Fire started on July 26, 2018 in Payette National Forest, Idaho and burned 14,000 ha of forest and rangelands before being contained on August 25, 2018. Burned Area Emergency Response (BAER)

teams identified 6000 ha of low, 6200 ha of moderate, and 450 ha of high soil burn severity areas (USDA Forest Service 2018). The vegetation is primarily Douglas fir/ninebark (*Pseudotsuga menziesii; Physocarpus malvaceus*) and ponderosa pine/bluebunch wheat grass (*Pinus ponderosa/Pseudoroegneria spicata*). The soils are loam to fine sandy loams (*Lithic and Typic Cryoborolls*, loamy skeletal, mixed; *Lithic Argiborolls*, loamy skeletal, mixed; and *Typic Cryochrepts*, fine, loamy, mixed) over Columbia River basalts with minor areas of intrusive Idaho Batholith granitic and metamorphosed gneiss and schist (USDA Forest Service 2018). The field soil sampling location for this study was in a high soil burn severity area as defined by Parson et al. (2010; Fig. 1). High water repellency was observed in the high soil burn severity areas only.

Bulk and intact soil core samples were collected from the surface soil in June 2019. In September 2019, an additional visit was made to collect soil core samples to a depth of 75 cm to determine the soil profile characteristics. Bulk soil was collected from the surface (0–10 cm depth) to a depth of 75 cm using shovels and 15-cm-long thin-walled samplers to determine field void ratio and water content at 15-cm intervals. Ash was still present and visible on the soil surface in June 2019. The 10-cm sample collection depth was selected to include wildfire ash and the soil that was directly affected by the wildfire heat. A 200-m^2 area classified as high soil burn severity was sampled evenly from the surface avoiding vegetation. The soil was passed through a custom sieve (1.27-cm opening diameter) in the field to remove gravel and large roots and brought to the laboratory for soil classification and rainfall simulation experiments. The bulk soil was again sieved (0.63-cm opening diameter) to homogenize the soil in the lab. Permission to obtain field soil samples was granted from the US Department of Agriculture Payette National Forest.

Atterberg limit and grain size distribution tests were performed to classify the soil according to the Unified Soil Classification System following ASTM D2487 (2017). Wet sieve results showed that the surface soil

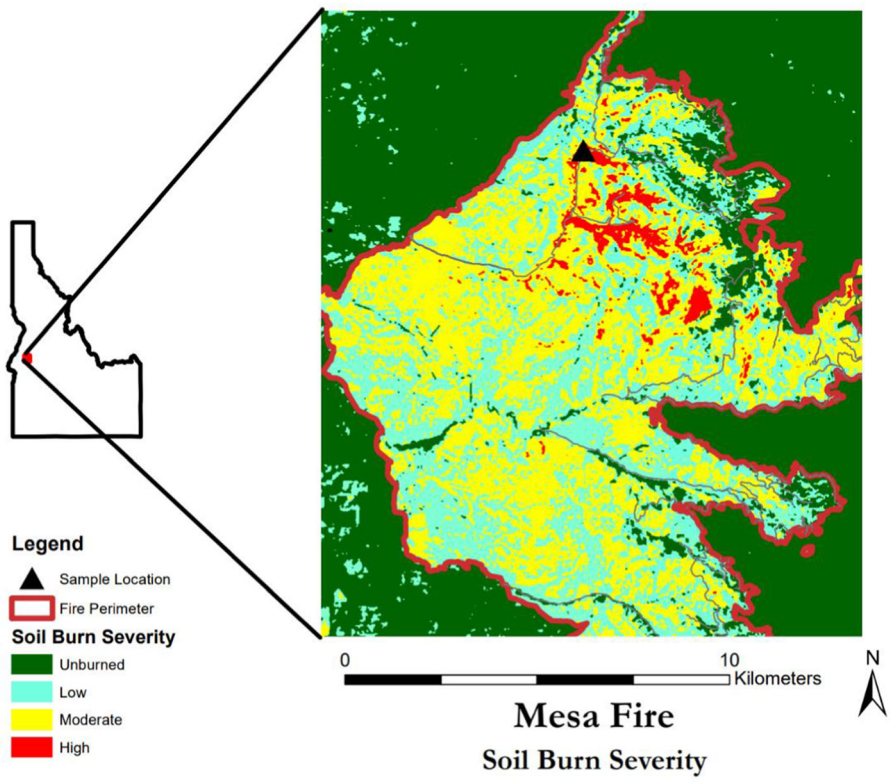

Fig. 1 Soil burn severity map of the 2018 Mesa Fire, Idaho

has 3% gravel, 34% sand, and 63% fines. It is classified as MH (liquid limit = 53, plasticity index = 11).

3 Rainfall Simulation Experiments

3.1 Experimental Setup

The rainfall simulation experiments were conducted at the US Department of Agriculture, Forest Service, Rocky Mountain Research Station rainfall simulation laboratory. Wildfire-burnt soil was compacted in custom-made plots following the methods of Pannkuk and Robichaud (2003), and successive wet-dry events were applied using a modified Purdue-type rainfall simulator (Meyer 1995) for wetting and ultraviolet (UV) lights for drying. The rainfall simulator uses the VeeJet nozzle, which provides energy of 275 kJ ha mm^{-1} at a 3-m height with an average drop diameter of 3 mm at a terminal velocity of 8.8 m sec^{-1} (Meyer and Harmon 1979). The custom-made plots are metal molds 68.5 cm in width and length and with a depth of 7 cm on the front side and a depth of 15 cm on the back side. The plots were aligned on a 45° slope using wooden frames and a wheeled platform for wetting (Fig. 2). Preliminary tests were performed with a 30° slope, but later the frames were adjusted to a 45° slope to test the effectiveness of the admixtures in a more critical condition. A plexiglass splash cover was attached to the collection trough (i.e., 7 cm deep) of the plots to minimize splash erosion (i.e., erosion caused by raindrops) at the transition from the plot to the collection trough and reduce rainfall to the measured surface. The collection trough was connected to sampling containers with rubber tubes. Figure 2a shows the test setup during wetting. For drying, the platforms were placed horizontally under two 5700-W UV light sources (Fig. 2b).

3.2 Compaction

The bulk soil that was sieved in the field (0.63-cm opening diameter) was brought to the target water content of 10% in the laboratory and compacted in the plots to the void ratio target of 2.1. The 2.1 void ratio was ensured in all the plots by controlling the dry mass of bulk soil compacted in the constant volume of the plots. Compaction was done solely to pack the soil in the plots at field void ratio, not to stabilize the soil. Therefore the void ratio was selected to represent the post-fire field conditions observed. The target compaction water content was selected to replicate the typical in situ water content experienced after a wildfire (Pannkuk and Robichaud 2003). The field soil was air-dried to 10% ± 5% water content prior to compaction. Compaction was done in three 3-cm layers using a custom 3.1-kg (150 mm by 150 mm) plate compactor. The compacted height of the soil was 9 cm, which exceeds the height of the collection trough of the plots by 2 cm. This was designed to allow eroded soil to travel into the collection trough without getting trapped at the front edge of the plots. After compaction, the surface of the plot was sealed

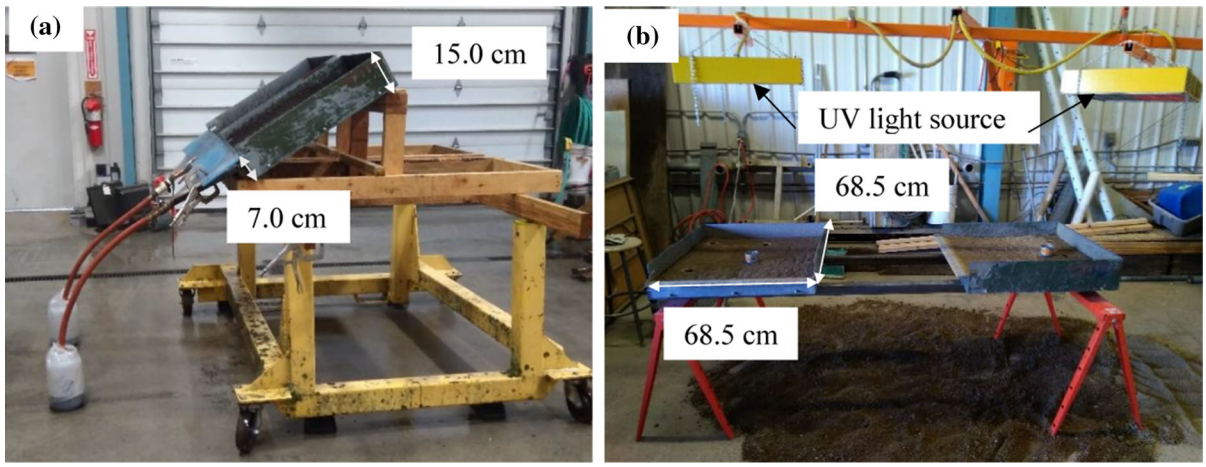

Fig. 2 Experimental setup during: **a** wetting and **b** drying events

with plastic sheeting to hold the moisture content constant until all the plots were compacted to field void ratio and ready for treatment application and rainfall simulation.

3.3 Treatment

Two admixtures were used for erosion treatment: xanthan gum (XG) and polyacrylamide (PAM). XG is a biopolymer, a polysaccharide produced via the fermentation of glucose or sucrose by the *Xanthomonas campestris* bacterium (Davidson 1978; Rosalam and England 2006). The structure consists of repeated units formed by five sugar residues: two glucose, two mannose, and one glucuronic acid (Jansson et al. 1975; Melton et al. 1976). $C_{35}H_{49}O_{29}$ is the fundamental chemical structure of XG. For this study, purified XG from Sigma-Aldrich (CAS 11138-66-2, St. Louis, MO) was used. PAM is a polymer with the basic structure of C_3H_5NO. A commercially available polymer (FLOBOND^{TM} A 30, SNF Inc, Riceboro, GA) was used in this study.

XG and PAM are both solid powders, and both were applied on the compacted soil surface using a sprinkling technique. Sprinkling would be the preferred technique in forest lands especially after a wildfire because of ease of application (i.e. helicopter or fixed wind aircraft) compared to mixing techniques with heavy machinery (Robichaud et al. 2013b). The treatments were applied carefully to accomplish uniform distribution over the surface. The surface of each soil in the plots (59.7 kg ha^{-1}) was sprinkled with 2.8 g of XG or PAM. The additive concentration was selected based on the recommendations of the PAM manufacturer and the same rate was selected for XG for comparison. Sprinkling, when applied to low-water-content soil (i.e., 10%), is a form of dry blending and results in a phase-separated structure in which the polymer coats the soil particles rather than getting into the interlayers (Alexandre and Dubois 2000; Akin and Likos 2016).

3.4 Rainfall, Runoff, Sediment Yields, and Drying

After compaction and treatment, the plots were placed on the wooden frames on elevated platforms. Rainfall was applied for 30 min at an intensity of 102 mm/h using the rainfall simulator. The application rate was selected to represent a high intensity rainfall condition seen in the region. The rate was approximately equal to the rainfall intensity of a 10-min rainfall event with a 5- to 10-year return period (Hanson and Pierson 2001) and is similar to other rainfall simulation experiments to determine postfire infiltration and erodibility characteristics (Robichaud 2000 after partial dryin). Runoff samples were collected in 5-min intervals in six 3.8-L plastic bottles, plus one sample after the rainfall had stopped but runoff was continuing. After wetting, the plots were moved under UV lights and dried for 4 h or 8 h. The different drying times were used to simulate real field conditions due to antecedent rainfall. After drying, the plots were returned to the platform for the next rainfall event. Three rainfall events were simulated, the first two of which were followed by drying events. Three rainfall events was selected to evaluate the erosion susceptibility during the first wet season after the wildfire under dry and wet conditions and after partial drying (Robichaud 2000). Disk-shaped samples (7-cm diameter, 2-cm thickness) were cored from the plots after each wetting or drying event to determine the water content.

3.5 Post-rainfall Tests

The mass of eroded soil and volume of runoff after each rainfall event and the water content before each wetting or drying event were measured. The sample bottles were weighed to determine both the runoff volume and the mass of eroded soil using calibrated beakers. After the weight measurement, the samples were oven-dried (105 °C) and the mass of eroded soil was measured. The water content before each event was calculated by oven-drying (105 °C, 48 h) core samples.

3.6 Statistical Analysis

Linear mixed-effects models were run (Littell et al. 2006) in SAS 9.4 (SAS Institute, Cary, NC) using sediment yield or runoff as the dependent variable from each wetting event, wetting event as a fixed effect, treatment as a random effect, and sample time as the repeated measure unit. Residuals met normality assumptions.

3.7 Water Retention Behavior

The soil water retention curve (SWRC) of the untreated soil was measured using a water potential meter incorporating the chilled-mirror dew point technique (WP4C, METER Group, Pullman, WA). Bulk soil was oven-dried (105 °C) and mixed with deionized water. The proportions, by mass, of deionized water and dry soil were controlled to achieve target saturations, S (i.e., between 10 and 80%, in 10% increments) at a void ratio of 2.1. The soil–water mixture was homogenized using a mortar and pestle and compacted into steel WP4C cups at a constant volume. The cups were sealed with plastic caps after compaction and equilibrated for 24 h before suction measurement.

A fully automated vapor sorption analyzer (VSA, METER Group, Pullman, WA) operating in dynamic dewpoint isotherm (DDI) mode was used to measure the water vapor sorption isotherms of the admixtures. Each admixture was oven-dried (40 °C) for 2 h prior to testing. One gram of each dried admixture was placed in a stainless steel VSA cup as a thin uncompacted layer covering the cup surface. The admixtures were brought to 3% relative humidity (RH) followed by an adsorption cycle up to 95% RH, followed by a desorption cycle back down to 3% RH in 1% RH increments and at a controlled temperature of 25 ± 0.2 °C. The VSA automatically controls the RH in the sample chamber by circulating vapor-saturated or desiccated air, and moves to the next RH increment after taking a sample mass measurement that corresponds to the chamber RH, which is measured using a chilled-mirror dew point sensor (Leong et al. 2003; Campbell et al. 2007).

4 Results and Discussion

4.1 Soil Profile

Void ratios varied with water content and depth (Fig. 3). The void ratio progressively decreased with depth. Three major reductions were observed, at 15 cm (from 2.15 to 1.36), at 45 cm (from 1.21 to 0.94) and at 60 cm (from 0.94 to 0.79). The top 15 cm was in the loosest state because of the presence of organics and environmental disturbance and was the most prone to soil loss. Therefore, a target void ratio of

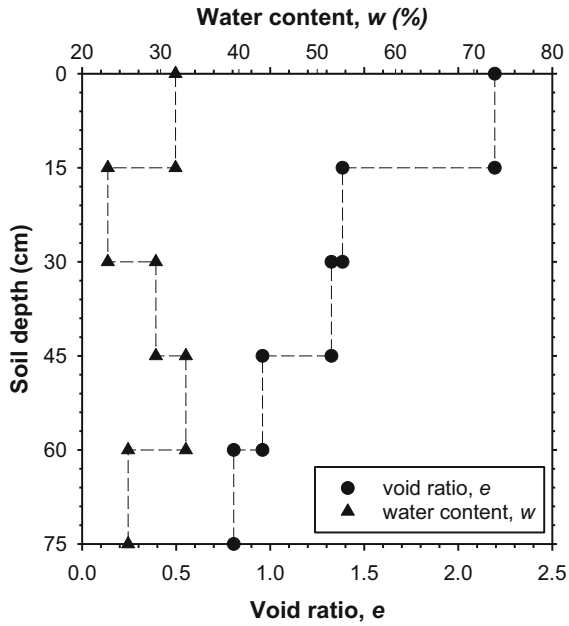

Fig. 3 Variation of water content and void ratio with soil depth for the untreated field soil

2.15 was selected for conducting rainfall simulation experiments. The water content (gravimetric) did not show a particular trend with depth and fluctuated between 23 and 33%.

4.2 Water Content Before Each Wet–Dry Event

Water content before each wetting or drying event was calculated (Fig. 4). The water contents before the second drying event are reported as approximate values (within 3%). The target compaction water content was 10%, but at the end of compaction before the first wetting event the measured water content varied slightly, between 9.3% and 10.6%. The first wetting event increased the water content to ~ 70% for untreated and to ~ 45% for PAM and XG plots. The second wetting event was applied when the water content of the untreated plot was at ~ 63% of saturation, and that of the PAM and XG plots were at ~ 31%. The second wetting event increased the water contents to ~ 68% (for untreated) and ~ 53% (for PAM- and XG-treated). The third wetting event was applied when the water contents were 29% for PAM, 33% for XG, and 36% for the untreated plot. The third wetting event increased the water contents of

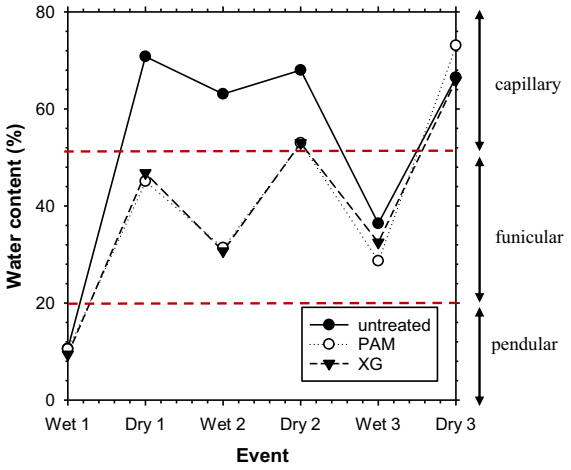

Fig. 4 Water content before each event and its relationship to retention regimes (i.e., pendular, funicular, capillary). Horizontal dashed lines indicate transitions between retention regimes. In capillary regime soil is saturated and has the maximum hydraulic conductivity, in funicular regime soil is unsaturated but the water phase is still continuous, in pendular regime water is in the form of thin films adsorbed on soil surface

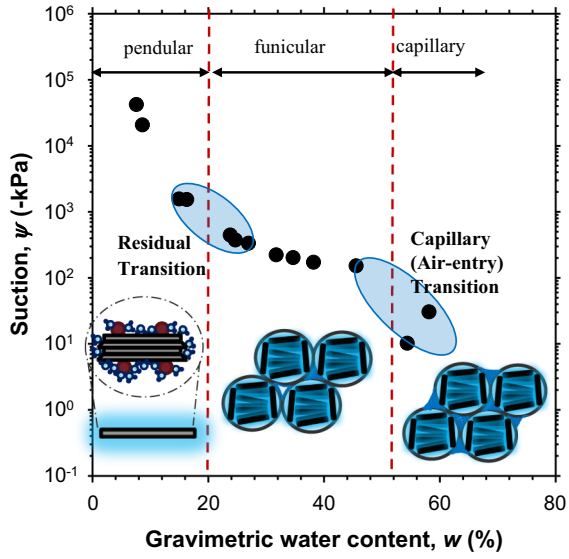

Fig. 5 Soil water retention curve of the untreated burnt soil from a surface sample and retention regimes. Red lines indicate transition in retention regimes. Insert images describe the location of water molecules in the soil system

untreated and XG plots to ~ 66% and that of PAM plots to ~ 73%.

The SWRC of the untreated soil was used to determine the locations of water molecules and the predominant water uptake mechanism before each event. Gravimetric water content (w) is used to present the SWRC for easy comparison with the water content values before each wetting or drying event (Fig. 5). The accuracy of WP4C measurements decrease at low suctions. Therefore, the last two data points are not expected to be fully accurate, however, the data presents the general trend in SWRC. The water retention regimes (pendular, funicular, and capillary regimes) and transition regions (residual and air-entry transition) are qualitatively marked on the SWRC together with sketches demonstrating the location of water molecules in each regime (Fig. 5). In the pendular regime, water molecules are adsorbed onto soil surfaces in the form of a thin layer. Hydration of external surfaces, cation hydration, hydration of internal surfaces and multilayer adsorption are the water uptake mechanisms in this regime (e.g., Kraehenbuehl et al. 1987; Cases et al. 1997; Keren and Shainberg, 1979; Ormerod and Newman 1983; Zhang and Lu 2018; Lu and Khorshidi 2015). Towards the end of the pendular regime, capillary condensation may start in mesopores (e.g., Akin and Likos 2017, 2020; Zhang and Lu 2018). Residual transition marks the switch from adsorption-dominated water uptake to a capillarity-dominated water uptake regime. Water molecules are condensed in mesopores and progressively in macropores as suction decreases. Capillary condensation is the predominant mechanism in this regime. In the capillary regime, the soil is saturated, but pore water pressures are still negative. For the untreated soil, the residual transition is at ~ 20% w and the capillary transition is at ~ 55% w. It should be noted that the transitions do not occur abruptly at a fixed water content, but rather occur over a range of w. The dashed lines mark a w from the midpoint of the transition areas. The residual (20% w) and air-entry (55% w) transitions are also marked to indicate the trends in w before each wetting or drying event (Fig. 4). Initially, soil in all three plots was unsaturated, in the pendular state. Between the first and third wetting events, the untreated soil stayed within the capillary regime, whereas PAM- and XG-treated soil stayed within the funicular regime. As expected, the third wetting event brought all three soils from the funicular regime to the capillary regime.

Both PAM- and XG-treated soils maintained lower water contents than the untreated soil because of additional interactions between water and the admixture. The only exception to this trend was at the end of

the third wetting event, when the water content of the PAM-treated soil was ~ 7% greater than that of the XG-treated soil and the untreated soil. Both PAM and XG form a hydrogel at high saturations, where water is retained by the hydrophilic functional groups of the hydrogel structure, which results in swelling (Qureshi et al. 2017; Tian et al. 2016; De et al. 2002). The water bound in a hydrogel structure is entrapped and immobile. As a result of the swelled hydrogel structure on the surface, infiltration was reduced for PAM and XG plots. Even though additional water was retained in the hydrogel structure, the low infiltration resulted in lower water contents in the PAM and XG plots than in the untreated plot at the ends of the first and second wetting events. The difference in water content between treatment alternatives was less at the end of the third wetting event, and this is attributed to the loss of PAM and XG with runoff over time.

4.3 Interaction of PAM and XG with Water

The interaction of PAM or XG with water molecules controls hydrogel formation and swelling and therefore the reduction in infiltration rates. Water vapor sorption isotherms of PAM and XG were used to evaluate the interactions. The hysteretic sorption isotherms of PAM and XG showed two distinct slopes, which represent the dominant water uptake mechanism, and a change in slope, which represents the transition region from adsorption to capillary condensation in mesopores (Fig. 6; Akin and Likos 2017). The milder slope, up to ~ 50% RH for PAM and up to ~ 80% RH for XG, represents the adsorption regime, where water is in the form of adsorbed films on the active surface sorption sites. As RH increases, there are two mechanisms that increase the slope of the isotherm: (1) onset of capillary condensation in mesopores and (2) onset of formation of the hydrogel structure. The transition occured at a lower RH for PAM, indicating that the PAM surface is less active than the XG surface initially, when the admixture is dry. However, at 95% RH, the amount of water adsorbed by PAM was ~ 1.8 times greater than that adsorbed by XG, indicating that the PAM hydrogel structure holds more water than XG.

After desorption, both XG and PAM formed a solid, crust-like structure (small images in Fig. 6). Shrinkage cracks and diameter reduction were apparent in XG, and diameter reduction due to shrinkage was apparent

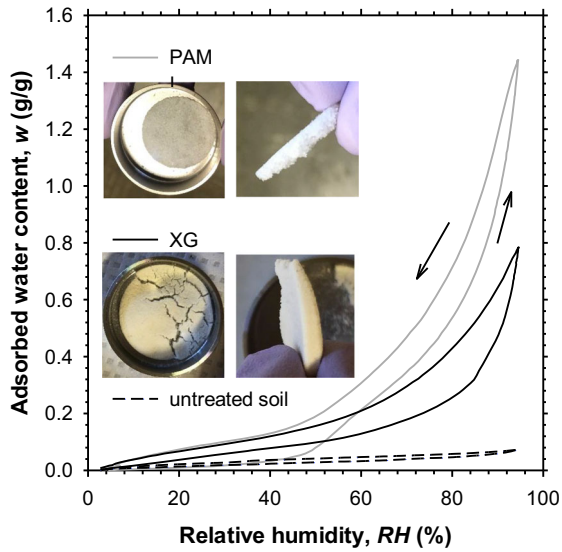

Fig. 6 Water vapor sorption isotherms of untreated soil, PAM and XG. Inset photos: PAM and XG specimens after a complete sorption cycle

in PAM. This shrinkage behavior indicates that both PAM and XG form a hydrogel structure at some RH along the adsorption curve that results in a volume increase. Note that the maximum adsorbed water contents are only 1.4 g/g (for PAM) and 0.8 g/g (for XG) at 95% RH, indicating that hydrogel formation can initiate without the presence of liquid water. For comparison, the maximum adsorbed water content of untreated surface soil is 0.073 g/g.

4.4 Runoff and Soil Loss

During the first 5 min of wetting, no runoff was observed, indicating that infiltration was increasing the soil saturation (Fig. 7). The trends in runoff for the untreated condition indicate that a transition occurred at ~ 20 min, at which point runoff started to increase. Both treatments caused the runoff to increase sooner in the run, 5 min for XG and 10 min for PAM treatments. Wetting cycle and treatment were not significant for predicting runoff.

The runoff from both XG- and PAM-treated plots was increased, though not significantly, in the first wetting event, to 2.8 times that of the untreated plot (Table 1). XG showed a consistent amount of runoff in all three wetting events, whereas PAM showed 50% more runoff during the second wetting event than in the third wetting event. The total runoff at the end of

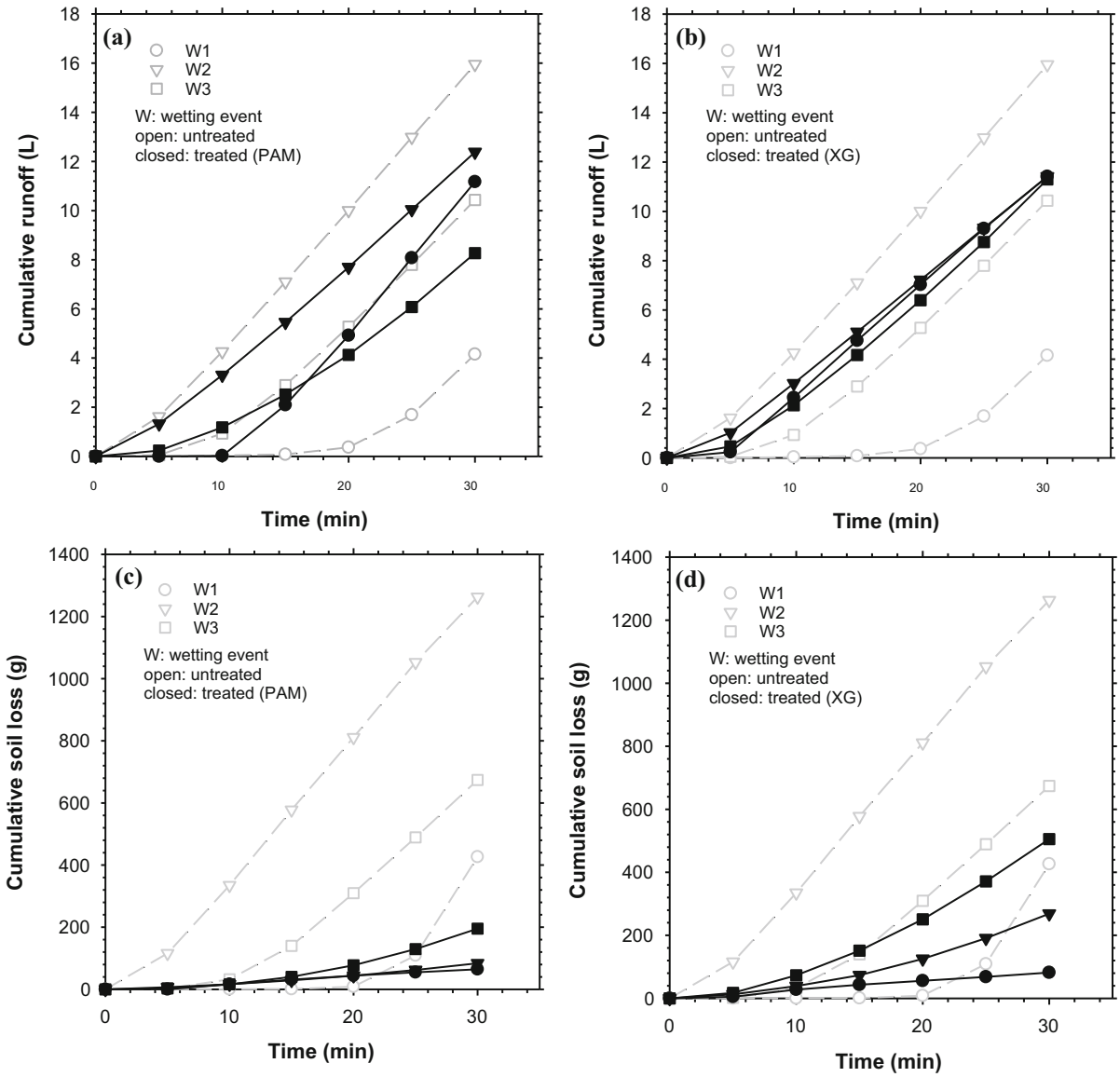

Fig. 7 Mean cumulative runoff and soil loss after each wetting event for **a**, **c** PAM and **b**, **d** XG in comparison with untreated soil. W indicates wetting event (1, 2, or 3). Data points indicate the sample were taken at 5-min intervals

Table 1 Mean soil loss and runoff values for the three wetting events by treatment from the samples collected (N = 27)

Treatment	Soil loss (g)	Runoff (L)
Untreated	112.6 a	1454 a
PAM	16.4 b	1515 a
XG	40.8 b	1624 a

Different lowercase letters within a column indicate significant difference by treatment at $\alpha = 0.05$

the three wetting events was increased by ~ 4% for PAM and ~ 12% for XG. The results indicate that both PAM and XG result in a small decrease (4–12%) in infiltration but neither seals the soil surface completely.

Soil loss from the untreated plot started at 20 min with a progressive increase in runoff (Fig. 7). The (a) PAM and (b) XG plots showed significantly less cumulative and mean soil loss during each cycle than the untreated plot (Table 1). For the untreated plot, the

first wetting event did not result in soil loss until ~ 20 min, and soil loss increased exponentially with time (Fig. 7). The second wetting event initiated soil loss immediately. The rate of soil loss doubled after 5 min and stayed constant during the remainder of the rainfall event. The third wetting event did not initiate measurable soil loss in the first 10 min, and soil loss increased linearly after 15 min. The trends in soil loss over time were analyzed with respect to runoff (Fig. 7c, d), water content before each wetting event (Fig. 4), and the corresponding regime in SWRC (Fig. 5). The soil was in the pendular regime before the first wetting event. In the pendular regime, the water phase is discontinuous and therefore the hydraulic conductivity is multiple orders of magnitude smaller than that of saturated soil. The first wetting event moved the soil into the capillary regime. The second wetting event started when the soil was in the capillary regime (~ 68% water content), where the soil is essentially saturated and has the maximum hydraulic conductivity. As a result, both runoff and soil loss started immediately. The maximum cumulative soil loss among all three wetting events was measured (about twice that of the third wetting event). The third wetting event started when the soil was in the funicular regime (~ 36% water content), in which the water phase is continuous but the soil is still unsaturated.

The trends in soil loss over time were similar for PAM- and XG-treated soil (Fig. 7). The first wetting event resulted in ~ 20 g of soil loss after 10 min, and this value stayed constant with further increases in time. The second and third wetting events showed increases in soil loss with time. The third wetting event caused the greatest loss (2.3 times greater than the second wetting event for PAM and 1.9 times greater than the second wetting event for XG) (Fig. 7c, d). For both PAM and XG, the soil loss in the first 5 min was insignificant (i.e., < 10 g) for all three cycles. SWRC regimes, sorption isotherms, and runoff trends can be used to determine the soil loss trends in treated soils. The first wetting event started when the treated soils were in the pendular regime, identical with the untreated soil. It brought the treated soils into the funicular regime, which resulted in them having more runoff than the untreated soil (~ 7 L more for PAM and XG). The decrease in water content and increase in runoff indicate that hydrogel was formed within the 5–10 min of the first wetting event and that this resulted in a reduction in hydraulic conductivity. The second wetting event started when the soils were in the funicular regime. Runoff started immediately with wetting, but at a slower rate for the first 5 min (i.e., ~ 1 L of runoff in 5 min). For XG, there was only slightly more runoff (< 1 L) than during the first wetting event. Both XG and PAM reduced soil loss and decreased runoff in the second wetting event, with PAM reducing soil loss ~ 3 times as much, indicating PAM bound soil particles more strongly than XG during the second wetting event. The third wetting event started when the soils were in the funicular regime and brought the soils into the capillary regime. The larger increase in water content (from ~ 30 to ~ 70%) than in the second wetting event (from ~ 30 to ~ 55%) is reflected in PAM having ~ 4 L less runoff but still more soil loss than during the second wetting event (more than twice as much), indicating that the binding between soil particles was weaker and the polymer might be washed off with runoff. The runoff trends with XG did not change, but the soil loss doubled compared to the second event, indicating that the polymer might be lost. The total soil loss was still lower than that of the untreated soil after the third wetting event.

Soil loss increased with each wetting event, with XG resulting in twice as much soil loss as PAM during the second and third wetting events (Fig. 7). The progressive increase in soil loss with each wetting event may be due to a loss of cementing agent with each wetting event as polymer is washed away by runoff. At the end of the third wetting event, the total soil loss (i.e., soil loss due to the first, second, and third wetting events combined) was: 2365 g (untreated plot), 850 g (XG-treated plot), or 345 g (PAM-treated plot). Both XG and PAM treatments increased the runoff volume in the first wetting event but resulted in a more consistent runoff volume between successive wetting events. At the end of three wetting events, the total runoff from the untreated plot was 30.5 L, that for PAM was 31.8 L, and that for XG was 34.1 L. The total runoff increased by ~ 4% for PAM and ~ 12% for XG. Each wetting event resulted in 23.9 L of rainfall on a plot. Therefore, the corresponding total infiltration was 41.3 L for untreated, 40.0 L for PAM, and 37.7 L for XG. The results indicate that both PAM and XG result in a decrease in infiltration, especially during the first wetting event, but neither seals the soil surface completely.

4.5 Admixture Effectiveness for Erosion Control

Admixture effectiveness was evaluated using two criteria: improvement in erosion resistance and change in infiltration (or runoff volume). The most effective admixture would result in an increase in erosion resistance without sealing the soil surface. PAM and XG significantly reduced the soil loss (total and after each cycle), PAM by 6.9 times and XG by 2.8 times, although their performance decreased with each wetting cycle. In actual field conditions, natural regeneration of vegetation contributes to reduced erosion over time (Robichaud et al. 2016) therefore the decrease in performance could have little long-term consequences. Both PAM and XG slightly increased runoff (PAM by 4% and XG by 12%), but not significantly at the end of three wetting events. The water content before each wetting cycle had the most control over total runoff and soil loss (Fig. 7). All plots had the lowest soil loss during the first wetting event, for which the initial water content was $\sim$ 10%, and nearly zero soil loss in the beginning of the first wetting event (20 min for untreated, 5 min for PAM and XG). As a result, the lowest runoff was seen during the first wetting event for all plots. The PAM and XG treatments resulted in more controlled changes in water content: the successive wet-dry cycles resulted in $\sim$ 30% w before the second and third wetting events. In contrast, the untreated plot had $\sim$ 60% w before the second wetting event, which resulted in the greatest soil loss, and $\sim$ 35% w before the third wetting event.

The results shown in this study for wildfire-burnt soils are consistent with the literature results in terms of erosion reduction. A number of studies evaluated XG as a stabilizer for improving resistance to erosion. Movasat and Tomac (2020) treated hydrophobic sand with XG and found a decrease in runoff-dominated erosion. Kavazanjian et al. (2009) tested the wind erosion resistance of XG-treated, poorly graded, nonplastic silty sand by wet-mixing XG with soil and found that soil loss was reduced from over 30% to as low as 0.02%. Chang et al. (2016) treated a residual low plasticity clay with XG and found that erosion was reduced from over 20% to as low as 0.1%. However, the change in infiltration rate was not evaluated in these previous studies. The results of this study show that XG is a potential alternative for improving erosion resistance in wildfire-burnt soils without sealing the soil surface completely.

PAM has been used for erosion control in unburned agricultural and forest lands (e.g., Foltz et al., 2009; Lentz and Sojka 1994). Studies found that PAM treatment increases aggregation in soils without sealing the soil surface or reducing the hydraulic conductivity (e.g., Terry and Nelson 1986; Bryan 1992; Shainberg et al. 1990). When applied on wildfire-burnt soil, PAM resulted in a 4% total runoff, indicating that the surface was not completely sealed. Therefore, PAM is also an alternative for improving erosion resistance in wildfire-burnt soils.

5 Summary, Conclusion and Future Directions

Two admixtures, XG and PAM, were used to stabilize soil burnt by the 2018 Mesa Fire. Runoff and soil loss were compared, and these results were compared with those for untreated burnt soil. Three rainfall events were simulated using indoor rainfall simulations. Runoff and soil loss were measured during each wetting event, and the admixtures were compared in terms of changes in runoff and soil loss. Both PAM and XG reduced soil erosion. At the end of three rainfall events, the soil erosion was reduced by 2.9 times for XG (850 g) and 6.9 times for PAM (345 g) compared to the soil loss in untreated soil (2365 g). The soil loss during each wetting event was dependent on the water content before wetting. PAM and XG maintained the water content consistently around 30% before the second and third wetting events, which resulted in a progressive increase in soil loss with each wetting event. In contrast, the water content of the untreated soil fluctuated between 68% (before the second wetting event) and 36% (before the third wetting event), resulting in twice as much soil loss during the second event as during the third event.

Future studies are needed to test the repeatability of the method and to find the optimum application rate for each admixture for decreasing soil loss to a manageable rate without decreasing infiltration.

Acknowledgements This work was funded by the US Department of Transportation through the Pacific Northwest Regional University Transportation Center (to IDA) and the US Department of Agriculture, Forest Service, Rocky Mountain Research Station (to PRR). We would like to thank Ivy Woltering, Austin Durglo, Mathew Lesiecki, Holly Brown,

Taiwo Akinleye, Andoni Alfaro Leránoz and Seth Tawiah for their assistance during field and laboratory work.

Data Availability The data is available from the corresponding author upon reasonable request.

Declarations

Conflict of interest The authors declare no conflict of interest.

References

Akin ID, Likos WJ (2016) Water vapor sorption of polymer-modified bentonites. In: Proceedings of Geo-Chicago 2016 technical papers, Reston, VA, ASCE. https://doi.org/10.1061/9780784480144.050

Akin ID, Likos WJ (2017) Implications of surface hydration and capillary condensation to strength and stiffness of compacted clay. J Eng Mech. https://doi.org/10.1061/(ASCE)EM.1943-7889.0001265

Akin ID, Likos WJ (2020) Suction stress of clay over a wide range of saturation. Geotech Geol Eng 38:283–296. https://doi.org/10.1007/s10706-019-01016-7

Alexandre M, Dubois P (2000) Polymer-layered silicate nanocomposites: preparation, properties and uses of a new class of materials. Mater Sci Eng 28:1–63

ASTM D2487-11 (2017) Standard practice for classification of soils for engineering purposes (unified soil classification system). Annual Book of ASTM Standards, ASTM International, West Conshohocken, PA

Bryan RB (1992) The influence of some soil conditioners on soil properties: laboratory tests on Kenyan soil samples. Soil Technol 5:225–247

Campbell GS, Smith DM, Teare BL (2007) Application of a dew point method to obtain the soil water characteristic. In: Schanz T (ed) Experimental unsaturated soil mechanics. Springer, Berlin, pp 71–77

Cannon SH, Gartner JE, Parrett C, Parise M (2003) Wildfire-related debris flow generation through episodic progressive sediment bulking processes, Western USA. In: Rickenmann D, Chen CL (eds) Proceedings of 3rd international conference, Debris-flow hazards mitigation—mechanics, prediction, and assessment, Davos, Switzerland, pp 71–82

Cases JM, Berend I, Francois M, Uriot JP, Michot LJ, Thomas F (1997) Mechanism of adsorption and desorption of water vapor by homoionic montmorillonite: 3—the Mg2+, Ca2+, Sr2+, and Ba2+ exchanged forms. Clays Clay Miner 45(1):8–22

Chang I, Im J, Cho G (2016) An environmentally-friendly geotechnical approach for soil erosion reduction using microbial biopolymers. GeoChicago 2016 technical papers

Davidson IW (1978) Production of polysaccharide by *Xanthomonas campestris* in continuous culture. FEMS Microbiol Lett 3:347–349

De S, Atluri N, Johnson B, Crone W, Beebe D, Moore J (2002) Equilibrium swelling and kinetics of pH-responsive hydrogels: models, experiments, and simulations. J Microelectromech Syst 11(5):544–555

DeBano LF (2000) The role of fire and soil heating on water repellency in wildland environments: a review. J Hydrol 231–232:195–206

DeBano LF, Neary DG, Folliott PF (1998) Fire's effects on ecosystems. Willey, New York

Dennison PE, Brewer SC, Arnold JD, Moritz MA (2014) Large wildfire trends in the western United States, 1984–2011. Geophys Res Lett 41:2928–2933

Doerr SH, Shakesby RA, Walsh RPD (2000) Soil water repellency—its causes, characteristics and hydrogeomorphological significance. Earth Sci Rev 51:33–65

Durgin PB (1985) Burning changes the erodibility of forest soils. J Soil Water Conserv 40:299–301

Foltz RB, Copeland NS, Elliot WJ (2009) Reopening abandoned forest roads in northern Idaho, USA: quantification of runoff, sediment concentration, infiltration, and interrill erosion parameters. J Environ Manage 90(8):2542–2550

Gabet EJ (2003) Post-fire thin debris flows: sediment transport and numerical modeling. Earth Surf Process Landf 28:1341–1348

Gartner JE, Cannon SH, Bigio ER, Davis NK, Parrett C, Pierce KL, Rupert MG, Thurston BL, Trebish MJ, Garcia SP, Rea AH (2005) Compilation of data relating to the erosive response of 606 recently burned basins in the Western US: US Geological Survey Open File Report 2005–1218. http://pubs.usgs.gov/of/2005/1218

Hanson CL, Pierson FB (2001) Characteristics of extreme precipitation and associated stream flow in the Reynolds creek experimental Watershed, Idaho. In: Proceedings of the 12th symposium on global climate change, American Meteorological Society, Boston, MA, pp J2.13–J2.16

Jansson PE, Kenne L, Lindberg B (1975) Structure of the exocellular polysaccharide from *Xanthomonas campestris*. Carbohyd Res 45:275–282

Kavazanjian E, Iglesias E, Karatas I (2009) Biopolymer soil stabilization for wind erosion control. In: International conference on soil mechanics and geotechnical engineering, pp 881–884. https://doi.org/10.3233/978-1-60750-031-5-881

Keren R, Shainberg I (1979) Water vapor isotherms and heat of immersion of Na/Ca-montmorillonite systems—II: mixed systems. Clays Clay Min 27:145–151

Kraehenbuehl F, Stoeckli HF, Brunner F, Kahr G, Muller-Vonmoos M (1987) Study of the water-bentonite system by vapour adsorption, immersion calorimetry and x-ray techniques: 1. Micropore volumes and internal surface areas, following Dubinin's theory. Clay Miner 22:1–9

Lax A, Garcia-Orenes F (1993) Carbohydrates of municipal wastes as aggregation factor soil. Soil Technol 6:157–162

Lentz RD, Sojka RE (1994) Field results using polyacrylamide to manage furrow erosion and infiltration. Soil Sci 158(4):274–282

Leong EC, Tripathy S, Rahardjo H (2003) Total suction measurement of unsaturated soils with a device using the chilled-mirror dew-point technique. Géotechnique 53(2):173–182

Littell RC, Milliken GA, Stroup WW, Wolfinger RD, Schabengerger O (2006) SAS for mixed models, 2nd edn. SAS Institute, Cary

Lu N, Khorshidi M (2015) Mechanisms for soil-water retention and hysteresis at high suction Range. J Geotech Geoenviron Eng 141(8):04015032

Mataix-Solera J, Cerda A, Arcenegui V, Jordan A, Zavala LM (2011) Fire effects on soil aggregation: a review. Earth Sci Rev 109:44–60

Melton LD, Mindt L, Rees DA, Sanderson GR (1976) Covalent structure of the polysaccharide from *Xanthomonas campestris*: evidence from partial hydrolysis studies. Carbohyd Res 46:245–257

Meyer LD (1995) Rainfall simulators for soil erosion research. In: Lal R (ed) Soil erosion research methods, Soil and Water Conserv. Soc., Ankeny, pp 83–105

Meyer LD, Harmon WC (1979) Multiple-intensity rainfall simulator for erosion research on row sideslopes. Trans Am Soc Agric Eng 22:100–103

Mills AJ, Fey MV (2004) Frequent fires intensify soil crusting–physiochemical feedback in the pedoderm on long-term burn experiments in South Africa. Geoderma 121:423–437

Movasat M, Tomac I (2020) Post-fire mudflow prevention by biopolymer treatment of water repellent slopes. GeoCongress 2020 technical papers, pp 170–178

Neary DG, Klopatek CC, DeBano LF, Folliott PF (1999) Fire effects on belowground sustainability: a review and synthesis. For Ecol Manag 122:51–71

Newcombe CP, MacDonald DD (1991) Effects of suspended sediments on aquatic ecosystems. N Am J Fish Manag 11:72–82

Ormerod EC, Newman ACD (1983) Water sorption on Ca-saturated clays: II. Internal and external surfaces of montmorillonite. Clay Miner 18:289–299

Pannkuk CD, Robichaud PR (2003) Effectiveness of needle cast at reducing erosion after forest fires. Water Resour Res 39(12):1333. https://doi.org/10.1029/2003WR002318

Parise M, Cannon SH (2012) Wildfire impacts on the processes that generate debris flows in burned watersheds. Nat Hazards 61:217–227

Parsons A, Robichaud P, Lewis S, Napper C, Clark J (2010) Field guide for mapping post-fire soil burn severity. Gen Tech Rep RMRS-GTR-243. Fort Collins, CO: US Department of Agriculture Forest Service, Rocky Mountain Research Station, 49 p

Peppin DL, Fule PZ, Sieg CH, Beyers JL, Hunter ME, Robichaud PR (2011) Recent trends in post-wildfire seeding in western US forests: costs and seed mixes. Int J Wildland Fire 20:702–708

Qureshi MU, Chang I, Al-Sadarani K (2017) Strength and durability characteristics of biopolymer-treated desert sand. Geomech Eng 12:785–801

Riechers GH, Beyers JL, Robichaud PR, Jennings K, Kreutz E, Moll J (2008) Effects of three mulch treatments on initial postfire erosion in North-Central Arizona, Gen technical report PSW-GTR-189. Albany, CA: US Department of Agriculture Forest Service, Pacific Southwest Research Station, pp107–113

Robichaud PR (2000) Fire effects on infiltration rates after prescribed fire in northern Rocky Mountain forests, USA. J Hydrol 231–232:220–229

Robichaud PR (2005) Measurement of post-fire hillslope erosion to evaluate and model rehabilitation treatment effectiveness and recovery. Int J Wildland Fire 14(4):475–485

Robichaud PR, Ashmun LE (2013) Tools to aid post-wildfire assessment and erosion-mitigation treatment decisions. Int J Wildland Fire 22:95–105

Robichaud PR, Beyers JL, Neary DG (2000) Evaluating the effectiveness of postfire rehabilitation treatments. General Technical Report RMRS-GTR-63, Fort Collins, CO: US Department of Agriculture, Forest Service, Rocky Mountain Research Station, 63 p

Robichaud PR, Lewis SA, Wagenbrenner LE, Ashmun LE, Brown RE (2013a) Post-fire mulching for runoff and erosion mitigation part I: effectiveness at reducing hillslope erosion rates. CATENA 105:75–92

Robichaud PR, Ashmun LE, Foltz RB, Showers CG, Groenier JS, Kesler J, DeLeo C, Moore M (2013b) Production and aerial application of wood shreds as a post-fire hillslope erosion mitigation treatment. General technical report RMRS-GTR-307. Fort Collins, CO: U.S. Forest Service, Rocky Mountain Research Station, 31p

Robichaud PR, Wagenbrenner JW, Pierson FB, Spaeth KE, Ashmun LE, Moffet CA (2016) Infiltration and interrill erosion rates after a wildfire in western Montana, USA. CATENA 142:77–88

Rosalam S, England R (2006) Review of xanthan gum production from unmodified starches by *Xanthomonas campestris* sp. Enzyme Microb Technol 39:197–207

Shainberg I, Warrington DN, Rengasamy P (1990) Water-quality and PAM interactions in reducing surface sealing. Soil Sci 149:301–307

Shakesby RA, Doerr SH (2006) Wildfire as a hydrological and geomorphological agent. Earth Sci Rev 74:269–307

Smith CJ, Caldwell J (2001) Salmon and steelhead habitat limiting factors in the Washington coastal streams of WRIA 21. Water resources inventory area 21 final report, Washington State Conservation Commission, 300 Desmond Drive, Lacey, WA 98503

Staley DM, Wasklewicz TA, Kean JW (2014) Characterizing the primary material sources and dominant erosional processes for post-fire debris-flow initiation in a headwater basin using multi-temporal terrestrial laser scanning data. Geomorphology 214:324–338

Staley DM, Negri JA, Kean JW, Laber JM, Tillery AC, Youberg AM (2017) Prediction of spatially explicit rainfall intensity-duration thresholds for post-fire debris flow generation in the western United States. Geomorphology 278:149–162

Terry RE, Nelson SD (1986) Effects of polyacrylamide and irrigation method on soil physical-properties. Soil Sci 141:317–320

Tian K, Likos WJ, Benson CH (2016) Pore-scale imaging of polymer-modified bentonite in saline solutions. Geo-Chicago 2016 technical papers, pp 468–477

USDA Forest Service (2018) Burned Area Report of the 2018 Mesa Fire, US Department of Agriculture, Forest Service, Payette National Forest, 15p. https://forest.moscowfsl.wsu.edu/BAERTOOLS/baer-db/2500-8/2500-8_Mesa%20Fire_Payette.pdf. Accessed 24 June 2020

Wagenbrenner JW, MacDonald LH, Rough D (2006) Effectiveness of three post-fire rehabilitation treatments in the Colorado Front Range. Hydrol Process 20:2989–3006

Wells WG (1987) The effect of fire on the generation of debris flows in southern California. In: Costa JE, Wieczorek GF (eds) Debris flows/avalanches: process, recognition, and

mitigation, GSA reviews in engineering geology, vol 7, pp 105–113
Westerling AL (2016) Increasing western US forest wildfire activity: sensitivity to changes in the timing of spring. Philos Trans R Soc B 371:20150178
Westerling AL, Hidalgo H, Cayan DR, Swetnam T (2006) Warming and earlier spring increases western US forest wildfire activity. Science 313:940–943
Wohlgemuth PM, Beyers JL, Robichaud PR (2011) The effectiveness of aerial hydromulch as an erosion control treatment in burned chaparral watersheds, Southern California. In: The fourth interagency conference on research in the watersheds, 26–30 September 2011, Fairbanks, AK, 6p
Wondzell SM, King JG (2003) Postfire erosional processes in the Pacific Northwest and Rocky Mountain regions. For Ecol Manage 178:75–87
Zhang C, Lu N (2018) What is the range of soil water density? Critical reviews with a unified model. Rev Geophys. https://doi.org/10.1029/2018RG000597